haematologica
Journal of the Ferrata Storti Foundation

Efficacy of the kinase inhibitor *CHZ868* against *JAK2* rearrangements in pediatric acute lymphoblastic leukemia

by Manuel Quadri, Claudia Saitta, Sonia Palamini, Stefano Rebellato, Titus Watrin, Jia-Wey Tu, Sanil Bhatia, Arndt Borkhardt, Chiara Palmi, Andrea Biondi, Giovanni Cazzaniga and Grazia Fazio

Received: May 8, 2025.
Accepted: April 9, 2026.

Citation: Manuel Quadri, Claudia Saitta, Sonia Palamini, Stefano Rebellato, Titus Watrin, Jia-Wey Tu, Sanil Bhatia, Arndt Borkhardt, Chiara Palmi, Andrea Biondi, Giovanni Cazzaniga and Grazia Fazio. Efficacy of the kinase inhibitor CHZ868 against JAK2 rearrangements in pediatric acute lymphoblastic leukemia.
Haematologica. 2026 Apr 16. doi: 10.3324/haematol.2025.287840 [Epub ahead of print]

Efficacy of the kinase inhibitor *CHZ868* against *JAK2* rearrangements in pediatric acute lymphoblastic leukemia

Manuel Quadri[1], Claudia Saitta[1,2], Sonia Palamini[1,2], Stefano Rebellato[1], Titus Watrin[3], Jia-Wey Tu[3], Sanil Bhatia[3], Arndt Borkhardt[3], Chiara Palmi[1], Andrea Biondi[1,4], Giovanni Cazzaniga[1,2*], Grazia Fazio[1,2*].

[1]Tettamanti Center, Fondazione IRCCS San Gerardo dei Tintori, Monza, Italy

[2]School of Medicine and Surgery, University of Milano-Bicocca, Italy

[3]Department of Pediatric Oncology, Hematology and Clinical Immunology, Medical Faculty, Heinrich Heine University Düsseldorf, Düsseldorf, Germany

[4]Pediatrics, Fondazione IRCCS San Gerardo dei Tintori, Monza, Italy

*Co-corresponding authors

Giovanni Cazzaniga (giovanni.cazzaniga@unimib.it) and Grazia Fazio (grazia.fazio@unimib.it), Via G. Pergolesi 33, 20900 Monza, Italy

Short Title

CHZ868 targets JAK2r in pediatric leukemia

DISCLOSURES

The authors declare no competing financial interests.

DATA SHARING STATEMENT

Original data are available from the corresponding authors on request.

CREDIT AUTHORSHIP CONTRIBUTION STATEMENT

Manuel Quadri: Conceptualization, Writing – Original Draft Preparation, Review & Editing, Investigation, Methodology, Formal Analysis, Validation, Visualization, Funding Acquisition. **Claudia Saitta**: Investigation, Methodology, Formal Analysis. **Sonia Palamini**: Investigation, Methodology, Formal Analysis. **Stefano Rebellato**: Investigation, Methodology, Formal Analysis. **Titus Watrin**: Methodology, Formal Analysis. **Jia-Wey Tu**: Methodology, Formal Analysis. **Sanil Bhatia**: Methodology, Formal Analysis. **Arndt Borkhardt**: Methodology, Formal Analysis. **Chiara Palmi**: Methodology, Formal Analysis, Funding Acquisition. **Andrea Biondi**: Resources. **Giovanni Cazzaniga**: Conceptualization, Writing – Review & Editing, Formal Analysis, Funding Acquisition, Project Administration, Supervision. **Grazia Fazio**: Conceptualization, Writing – Review & Editing, Formal Analysis, Funding Acquisition, Project Administration, Supervision. All authors read and approved the final version of the manuscript.

SOURCES OF FUNDING

This work was supported by Fondazione AIRC per la ricerca sul cancro (project numbers 2022-28342 to M.Q. and IG2023-29191 to G.F.), the Italian Ministry of Health, Fondazione Cariplo (project number 2018-0339 to C.P. and supporting M.Q. fellow). S.B. was supported by the “Elterninitiative Kinderkrebsklinik e.V.”. A.Bo. was supported by the “Katharina-Hardt-Foundation, Bad Homburg, Germany”. We deeply thank “Fondazione Maria Letizia Verga” for supporting M.Q. and the research project. We thank Novartis that signed the MTA to provide us with CHZ868.

MAIN TEXT

B-cell precursor acute lymphoblastic leukemia (BCP-ALL) is the most frequent subtype of acute lymphoblastic leukemia (ALL), the most common pediatric cancer.[1] Nowadays the improvement of chemotherapy protocols led patients to an event free survival of 85%, while 15% of patients still relapse, with only 20-45% cure rate by second line therapies.[2] The group named Philadelphia-like (Ph-like) or BCR::ABL1-like[3], recently included in the WHO as associated to high-risk of relapse,[4] has been defined to have a genetic expression pattern similar to Philadelphia-positive ALL, despite not having the underlying *BCR::ABL1* fusion. In 90% of cases alterations of *ABL1/ABL2*, *PDGFRB/A, CSF1R, CRLF2*, *PAX5*, *EPOR*, and *JAK2* genes are included in this subgroup.[5-6]

JAK2 is a non-receptor tyrosine kinase, involved in hematopoiesis, signaling pathways and cellular processes, and known to be deregulated in leukemias, lymphomas and myeloproliferative neoplasms.[4,7] *JAK2* rearrangements (JAK2r) are found in 5% of pediatric Ph-like ALL[4,5,8], representing an appealing target of tyrosine kinase inhibitors (TKIs)[4]. In the last years, the production of type-II TKIs has increased, as they could overcome the limits of type-I TKIs by targeting the JAK2 active form. Ruxolitinib is the most used type-I TKI, but despite its efficacy, also in combination approaches, it showed some limitations, as hyperphosphorylation of JAK2/STATs and loss of response that determine the "paradoxical effect" of increasing JAK2 activation.[9-10] Vice versa, type-II TKIs bind their target in the inactive conformation, covering regions adjacent to the ATP-binding site, with an advantage in efficacy.[11] Interestingly, the novel type-II TKI CHZ868 showed promising results *in-vitro* and *in-vivo*, in presence of *CRLF2* rearrangements in BCP-ALL PDXs.[9,11] The preliminary CHZ868 efficacy prompted us to develop the present preclinical study with the aim of targeting JAK2r in pediatric BCP-ALL.

Primary samples of pediatric patients affected by BCP-ALL have been collected and analyzed, in accordance with the ethical standards of the Declaration of Helsinki and following national and international guidelines. We applied the Next Generation Sequencing (NGS) RNA target capture strategy implementing either the Illumina TruSight RNA Pan-Cancer Library Prep or the Nugen

Custom Panel, as previously described[12]. An *in-vivo* Patient-Derived-Xenograft (PDX) model has been set up in immunodeficient NOD.Cg-Prkdc^{scid} Il2rg^{tm1Wjl}/SzJ (NSG) mice to expand primary patients' bone marrow (BM) samples. Cells derived from PDXs were both co-cultured on a layer of human bone marrow stroma (HBMS) for apoptosis/viability assays and analyzed by HTP drug screening, as previously described.[6,13] Phosphoflow on PDXs-derived blasts was performed at basal level or after drugs treatment.[6] We treated PDXs with leukemic blasts carrying *PAX5::JAK2*, *ATF7IP::JAK2* or *ZEB2::JAK2* fusions, with either CHZ868 or vehicle. After *in-vivo* treatment, whole transcriptome analysis has been performed by Universal RNAseq kit and FASTQ files are available in the BioStudies database (https://www.ebi.ac.uk/biostudies/) under accession E-MTAB-15657.

12 pediatric JAK2r cases (mean age=9.6 years) were identified by RNAseq screening of 895 (1.3%) BCP-ALL pediatric patients at diagnosis (**Supplemental figure 1A**). *ZEB2::JAK2*, *GIT2::JAK2*, *TLE4::JAK2* and *MPRIP::JAK2* were validated as novel fusions, beside the known *BCR::JAK2*, *ATF7IP::JAK2* and *PAX5::JAK2* (6/12 cases). In all cases, *JAK2* maintains its kinase domain at the 3', joined with the 5' partner gene (data not shown).

We developed PDXs from 3 representative patients, carrying *PAX5::JAK2* (patient 1), *ATF7IP::JAK2* (patient 2) and *ZEB2::JAK2* (patient 3) fusion, respectively (**Supplemental figure 1B-C**).

The constitutive basal phosphorylation of Y1007-1008 residues in the loop of activation of JAK2 in all three JAK2r cases was significantly higher than the negative controls. *PAX5::JAK2* and *ZEB2::JAK2* had also higher pJAK2 than positive controls, known to have an active JAK/STAT pathway, while in *ATF7IP::JAK2* pJAK2 was comparable to positive controls (range +17%/+70%, $0.05<p<0.01$) (**Supplemental figure 1D**). JAK2 constitutive activation induced the basal activation of pSTAT5(Y694) in all JAK2r, while no difference in pSTAT3(S727) expression was found among PAX5::JAK2, positive and negative controls, whereas pSTAT3 was unexpectedly significantly higher in ATF7IP::JAK2 and ZEB2::JAK2 (**Supplemental figure 1D).**

CHZ868 monotherapy treatment (up to 60 minutes), given at 50% lethal dose (LD50) patient-specific doses (**Figure 1A**), showed a higher specificity and efficacy towards pJAK2(Y1007-1008) than ruxolitinib monotherapy treatment (30 minutes: CHZ868 -33%/-71%, $0.01<p<0.001$ vs ruxolitinib 5%/-24%, $ns<p<0.05$). Vice versa, ruxolitinib showed higher efficacy on pSTAT5 than CHZ868 (30minutes: ruxolitinib -27%/-62%, $0.05<p<0.01$ vs CHZ868 -12%/-52%, $0.05<p<0.01$). Interestingly, both drugs had a comparable significant effect on pSTAT3. The % of reduction is indicated as a range of the 3 patients analyzed.

After 48h treatment with CHZ868 or ruxolitinib of blasts in co-culture on a layer of HBMS, ruxolitinib showed no effect on pJAK2 on both *PAX5::JAK2* and *ATF7IP::JAK2,* while inhibiting pSTAT5 only in *ATF7IP::JAK2* and *ZEB2::JAK2*. Instead, *ATF7IP::JAK2* and *ZEB2::JAK2* showed a significant decrease in pJAK2 (-25%/-50%, $0.01<p<0.001$) and pSTAT5 (-20%/-65%, $0.001<p<0.0001$) after CHZ868 treatment. Even though pJAK2 was significantly reduced (-40%, $p<0.001$), pSTAT5 became hyperphosphorylated in *PAX5::JAK2* after both CHZ868 (+200%, $p<0.001$) and ruxolitinib (+50%, $p<0.001$) treatment. To note, both drugs had a strong effect on pSTAT3 (-50%, $p<0.0001$) only in *ATF7IP::JAK2,* a new observation for JAK2 inhibition in BCP-ALL (**Figure 1B**). Overall, CHZ868 and ruxolitinib significantly (and similarly) inhibited PI3K-AKT pathway's effectors (**Figure 1C**).

After 48h of CHZ868 treatment in combination with dexamethasone and ruxolitinib, a statistically significant and synergistic effect was assessed at LD50 dosage with ruxolitinib in *ATF7IP::JAK2* and *ZEB2::JAK2*, while the combination was additive in *PAX5::JAK2* (-62%/-90%, $0.01<p<0.001$). While *ATF7IP::JAK2* and *ZEB2::JAK2* showed resistance to dexamethasone, *PAX5::JAK2* resulted sensitive, as also supported by the statistically significant synergy between dexamethasone and CHZ868 (-95%, $p<0.001$). While CHZ868 did not overcome dexamethasone resistance in *ATF7IP::JAK2,* a synergistic effect was observed in *ZEB2::JAK2,* as in ruxolitinib and dexamethasone combination **(Figure 1D and supplemental figure 1E).**

Moreover, we confirmed PI3K pathway activation, downstream LCK, which is a known target of PAX5,[6] in *PAX5::JAK2* (**Supplemental figure 1F-L**). We further demonstrated that the triple kinase inhibitor nintedanib (BIBF1120)[6] is efficacious on *PAX5::JAK2* blasts on HBMS, both by the inhibition of PI3K-AKT pathway effectors (**Supplemental figure 2A**) and by its apoptosis induction, with an additive effect in combination with both CHZ868 (-64%, $p<0.001$) and ruxolitinib (-50%, $p<0.05$)(**Figure 1E).** Bliss score and combination index of drugs' combinations are reported in **supplemental figure 2B.** We also assessed the specific action of drugs on negative (w/o fusions) and positive controls (CRLF2r/JAK2m and CRLF2r only) (**Supplemental figure 2C-E**).

To resolve the ruxolitinib efficacy limited to high dosages, with loss of specificity towards pJAK2, we applied an *ex-vivo* high-throughput drug screening with alternative 174 inhibitors, including 110 FDA/EMA approved drugs, as previously described[13]. *PAX5::JAK2, ATF7IP::JAK2, ZEB2::JAK2* and *GIT2::JAK2* PDXs were tested, aiming to identify additional compounds to be combined with CHZ868 with synergistic effect. After 72 hours of treatment (8nM to 25uM), we compared the differential drug sensitivity score (dDSS)[14] of the JAK2r PDXs with MUTZ5 cell line (CRLF2r and JAK2m) and healthy donors (T cells and PBMCs). As reported in **Figure 2A**, among JAK2r PDXs, *PAX5::JAK2* PDX derived blasts were the most sensitive to several drugs, including currently used drugs in the AIEOP-BFM ALL 2017 pediatric protocol, and JAK TKIs. We identified drugs not belonging to selective JAK inhibitors, but specific for the JAK2r cohort and safe on healthy controls, such as birinapant (Smac mimetic, $p<0.05$). Among the JAK TKIs, ruxolitinib was not effective on JAK2r, while AT9283 was the most specific and effective on JAK2r ($p<0.05$), with no effect either on MUTZ5 or healthy controls. In 48h *ex-vivo* HBMS co-culture of three JAK2r PDXs, AT9283 combined with CHZ868 exerted a significant increase in the apoptotic effect compared to monotherapy ($p<0.0001$, **figure 2B and supplemental figure 2F**) with synergistic (in *PAX5::JAK2, ZEB2::JAK2*) or additive (in *ATF7IP::JAK2*) effect at LD50 (**Supplemental figure 2G).** To note, not only CHZ868 (range 8nM-25μM) demonstrated to be non-toxic on hematopoietic

stem and progenitor cells (HSPCs, $CD34^+$) (**Supplemental figure 2H**), but we also demonstrated the safety of AT9283, ruxolitinib and birinapant, on HSPCs purified from healthy donors, having a DSS<10, determined as cut-off for safety/toxicity evaluation[13] (**Figure 2C**).

We also demonstrated the *in-vivo* efficacy of CHZ868 in three JAK2r PDX models. First, all the three JAK2r CHZ868-treated mice groups showed a significant reduction of pJAK2 (-18%/-30%, $p<0.05$) and pSTAT5 (-23%/-45%, $p<0.05$) (**Supplemental figure 2I**), while PI3K pathway was not affected (**Supplemental figure 2L**). Importantly, after the two weeks of treatment at 30mg/kg, we detected a statistically significant reduction of the $hCD10^+CD19^+$ percentage of blasts in the hematopoietic organs, as bone marrow (-43%/-85%, $0.05<p<0.01$), spleen (-72%/-89%, $0.05<p<0.00001$) associated to spleen weight reduction (-37%/-60%, $0.001<p<0.00001$), and peripheral blood (-46%/-80%, $p<0.05$) (**Figure 2D and supplemental figure 3A**).

To deeply understand the CHZ868 mechanism of action downstream JAK2r, we performed whole transcriptome NGS on RNA extracted from CHZ868-treated vs. vehicle-treated mice (**Supplemental figure 3B**). The TKI treatment reduced *JAK2* expression in CHZ868-treated mice (**Supplemental figure 3C**) and KEGG analysis indeed confirmed downregulation of JAK/STAT signaling and pluripotency of stem cells pathways; however, different metabolic pathways were activated, as part of blasts metabolic rewiring (**Figure 3A**). By Hallmark GSEA, we observed an enrichment in MYC targets and metabolic rewiring (MTORC1 signaling, glycolysis and unfolded protein response), while JAK/STAT3/STAT5 signaling, KRAS signaling and inflammatory responses resulted downregulated (**Figure 3B**). We confirmed a cell cycle arrest of CHZ868-treated blasts as a consequence of proliferation suppression (downregulation of *RB1*, *E2F7/8*, *CCNE1/2*, *CDC25B* and *MKI67*) due to DNA damage (upregulation of *TP53* and *CDKN1A*) induced by JAK/STAT inhibition, conferring a quiescent state (upregulation of *ORC5* and *CCND3*) (**Figure 3C and supplemental figure 3D**). Since DNA damage was previously demonstrated to induce strong NF-kB activation, we indeed confirmed that CHZ868 treatment led to upregulation of canonical NF-kB pathway (upregulation of *IKBKB* and *TNFRSF1A*; downregulation of *CYLD*, *NFKBIE* and

RELB), denoted by immune evasion or reduced inflammation (downregulation of *TLR2/7*, *IL1RAP* and *TNFRSF11A*) with dominance of anti-apoptotic stimuli (upregulation of *BCL2* and *BIRC3*) (**Figure 3D and supplemental figure 3E**). Furthermore, we confirmed that the differentially expressed genes were indeed more correlated to anaerobic metabolic rewiring in stress conditions (ribosomal machinery, mitochondrial biogenesis, amino acids metabolism) rather than proliferation (**Supplemental figure 3F**).

In this study on a limited cohort of *JAK2*-rearraged cases, we aimed at exploring the targeting of *JAK2* rearrangements in leukemia by using the murine expansion of primary blasts from patients as a preferential model over cell lines, a limiting and confounding model. We demonstrated in our preclinical model that JAK2r PDXs have constitutive basal activation of JAK2/STAT5 pathway, that can be efficiently targeted both in *ex-vivo* and *in-vivo* treatment by CHZ868, a novel type-II TKI, in addition to a not usually described pSTAT3 downregulation after JAK2 inhibition in JAK2r. CHZ868, already effective *ex-vivo* at 100-fold lower dosages than ruxolitinib, the most used TKI, proved to induce apoptosis in synergic or additive combination with other kinase inhibitors, standard chemotherapy or CAR-T cell therapy[15]. CHZ868 was even able to overcome dexamethasone monotherapy resistance in a model recapitulating 2D BM niche.

Moreover, our HTP drug screening showed JAK2r PDXs sensitivity to other classes of drugs, as venetoclax (BCL2i) and omaveloxolone (NF-kBi), which may be used to target activated vulnerabilities (BCL2, effectors of NF-kB pathway) due to CHZ868-induced DNA damage. Combinatorial approaches of type-II JAK2i would be beneficial in clinics to overcome eventual limitations or resistance mechanisms induced by TKIs treatment. Importantly, the proposed drugs and compounds proved to be non-toxic on healthy cells, including HSPCs, thus supporting their potential use in JAK2r BCP-ALL in combination with clinically optimized type-II TKIs, not included in this study.

Although CHZ868 itself is not clinically developable due to unfavorable pharmacokinetic properties, our findings provide proof-of-principle evidence that type-II JAK2 inhibition is highly

effective in *JAK2*-rearranged pediatric BCP-ALL. Our data support further preclinical and clinical development of clinically suitable type-II JAK2 inhibitors for this high-risk subgroup.

ABBREVIATIONS

Acute lymphoblastic leukemia, ALL; B-cell-precursor acute lymphoblastic leukemia, BCP-ALL; Bone Marrow, BM; CHZ868, CHZ; *CRLF2* rearrangements, CRLF2r; dexamethasone, DEXA; Differential Drug Sensitivity Score, dDSS; Drug Sensitivity Score, DSS; Human bone marrow stroma, HBMS; Hematopoietic Stem and Progenitor Cells, HSPCs; *JAK2* mutation, JAK2m; *JAK2* rearrangements, JAK2r; 50% lethal dose, LD50; Meninges of central nervous system, CNS; Next Generation Sequencing, NGS; Nintedanib, BIBF1120; NOD.Cg-Prkdc^{scid} Il2^{rgtm1Wjl}/SzJ, NSG; Patient Derived Xenografts, PDXs; *PAX5* rearrangements, PAX5r; ruxolitinib, RUXO; Spleen, SP; Tumor cells, blasts; tyrosine kinase inhibitors, TKIs; Peripheral Blood, PB.

REFERENCES

1. Inaba H, Pui CH. Advances in the Diagnosis and Treatment of Pediatric Acute Lymphoblastic Leukemia. J Clin Med. 2021;10(9):1926.
2. Conter V, Aricò M, Basso G, et al. Long-term results of the Italian Association of Pediatric Hematology and Oncology (AIEOP) Studies 82, 87, 88, 91 and 95 for childhood acute lymphoblastic leukemia. Leukemia. 2010;24(2):255-264.
3. Den Boer ML, van Slegtenhorst M, De Menezes RX, et al. A subtype of childhood acute lymphoblastic leukaemia with poor treatment outcome: a genome-wide classification study. Lancet Oncol. 2009;10(2):125-134.
4. Tran TH, Tasian SK. Has Ph-like ALL Superseded Ph+ ALL as the Least Favorable Subtype? Best Pract Res Clin Haematol. 2021;34(4):101331.
5. Shiraz P, Payne KJ, Muffly L. The Current Genomic and Molecular Landscape of Philadelphia-like Acute Lymphoblastic Leukemia. Int J Mol Sci. 2020;21(6):2193.
6. Fazio G, Bresolin S, Silvestri D, et al. PAX5 fusion genes are frequent in poor risk childhood acute lymphoblastic leukaemia and can be targeted with BIBF1120. EBioMedicine. 2022;83:104224.
7. Downes CE, McClure BJ, McDougal DP, et al. JAK2 Alterations in Acute Lymphoblastic Leukemia: Molecular Insights for Superior Precision Medicine Strategies. Front Cell Dev Biol. 2022;10:942053.
8. Tasian SK, Hurtz C, Wertheim GB, et al. High incidence of Philadelphia chromosome-like acute lymphoblastic leukemia in older adults with B-ALL. Leukemia. 2017;31(4):981-984.
9. Tvorogov D, Thomas D, Liau NPD, et al. Accumulation of JAK activation loop phosphorylation is linked to type I JAK inhibitor withdrawal syndrome in myelofibrosis. Sci Adv. 2018;4(11):eaat3834.
10. McLornan DP, Pope JE, Gotlib J, Harrison CN. Current and future status of JAK inhibitors. Lancet. 2021;398(10302):803-816.
11. Wu SC, Li LS, Kopp N, et al. Activity of the Type II JAK2 Inhibitor CHZ868 in B Cell Acute Lymphoblastic Leukemia. Cancer Cell. 2015;28(1):29-41.
12. Grioni A, Fazio G, Rigamonti S, et al. A Simple RNA Target Capture NGS Strategy for Fusion Genes Assessment in the Diagnostics of Pediatric B-cell Acute Lymphoblastic Leukemia. Hemasphere. 2019;3(3):e250.
13. Oikonomou A, Valsecchi L, Quadri M, et al. High-throughput screening as a drug repurposing strategy for poor outcome subgroups of pediatric B-cell precursor Acute Lymphoblastic Leukemia. Biochem Pharmacol. 2023;15:115809.

14. Yadav B, Pemovska T, Szwajda A, et al. Quantitative scoring of differential drug sensitivity for individually optimized anticancer therapies. Sci Rep. 2014;4:5193.
15. Mitsuno K, Suematsu M, Naito Y, et al. Selective JAK2 pathway inhibition enhances anti-leukemic functionality in CD19 CAR-T cells. Cancer Immunol Immunother. 2025;74(3):79.

FIGURES LEGEND

Figure 1. Targeting of *JAK2* rearranged PDXs with tyrosine kinase inhibitors from short time points to 48h in co-culture on HBMS, to evaluate both the phosphorylation levels on JAK2/STATs and PI3K-AKT pathways by phosphoflow, and *ex-vivo* apoptosis/viability assays of combination of pairs of drugs, given at three different dosages for 48h on *PAX5::JAK2* blasts in co-culture with HBMS. Viability was assessed by Annexin V/7AAD staining (Annexin V/7AAD double negative hCD10$^+$ blasts). A. Heatmap representing the ratios of mean fluorescence intensity (MFI) of CHZ868-treated (LD50 dosage) or ruxolitinib-treated (LD50 dosage) on vehicle-treated hCD10$^+$ blasts of pJAK2 (Y1007-1008), pSTAT5 (Y694) and pSTAT3 (S727), at short time points (5' to 60') of treatment on PDX-derived blasts carrying a *PAX5::JAK2* fusion (left three columns), on PDXs-derived blasts carrying a *ATF7IP::JAK2* fusion (central three columns) and on PDX-derived blasts carrying a *ZEB2::JAK2* fusion (right three columns). N=3 experiments. Error bars represent standard deviation. Student's T test is shown as p values: *p<0.05; **p<0.01; ***p<0.001. Statistics reported in white refers to a significant reduction of phosphorylation in treated blasts compared to untreated blasts, while statistics reported in black refers to a significant increase of phosphorylation in treated blasts compared to untreated blasts. The internal control is represented by untreated cells (0 min). **B.** Heatmap representing MFI ratios of 48h TKIs-treated on vehicle-treated hCD10$^+$ PDX-derived blasts on HBMS co-culture carrying a *PAX5::JAK2* fusion (left three columns), on PDXs-derived blasts carrying a *ATF7IP::JAK2* fusion (central three columns) and on PDX-derived blasts carrying a *ZEB2::JAK2* fusion (right three columns) reporting the inhibition of pJAK2 (Y1007-1008), pSTAT5 (Y694) and pSTAT3 (S727). N=3 experiments, in technical duplicate. Error bars represent standard deviation. Student's T test is shown as p values: *p<0.05; **p<0.01; ***p<0.001. Statistics reported in white refers to a significant reduction of phosphorylation in treated blasts compared to untreated blasts, while statistics reported in black refers to a significant increase of phosphorylation in treated blasts compared to untreated blasts. The internal control is represented by untreated cells. **C.** Heatmap representing MFI ratios of 48h TKIs-treated on vehicle-treated hCD10+ PDX-derived blasts on HBMS co-culture carrying a *PAX5::JAK2* fusion (left five columns), on PDXs-derived blasts carrying a *ATF7IP::JAK2* fusion (central five columns) and on PDX-derived blasts carrying a *ZEB2::JAK2* fusion (right five columns) reporting the inhibition of PI3K-AKT pathway effectors [PDPK1, pAKT (S473), pAKT (T308), 4pEBP1, pS6]. N=3 experiments, in technical duplicate. Error bars represent standard deviation. Student's T test is shown as p values: *p<0.05; **p<0.01; ***p<0.001, ****p<0.0001. The internal control is represented by untreated cells. Statistics reported in white refers to a significant reduction of phosphorylation in treated blasts compared to untreated blasts, while statistics reported in black refers to a significant increase of phosphorylation in treated blasts compared to untreated blasts. The internal control is represented by untreated cells. **D.** *Ex-vivo* viability of hCD10$^+$ PDX-derived blasts on HBMS co-culture after 48h drugs combinations on *PAX5::JAK2* positive blasts, indicating the decrease of viable blasts while increasing the dosages (CHZ868: 0.193µM, 0.270µM, 0.347µM; ruxolitinib: 24µM, 32µM, 40µM; dexamethasone: 5ng/mL, 7ng/mL, 9ng/mL). Viability was assessed from apoptosis and necrosis after staining with Annexin V-PE/7AAD and expressed as decrease of the percentage of hCD10$^+$ viable blasts (Annexin V-PE/7AAD double negative cells) and expressed as percentage of viability on untreated cells. N=3 experiments, in technical duplicate. Error bars represent standard deviation. The internal control is represented by untreated (ut) cells. Student's T test is shown as p values: *p<0.05; **p<0.01; ***p<0.001, ****p<0.0001. **E.** *Ex-vivo* viability of hCD10$^+$ *PAX5::JAK2* blasts in co-culture on HBMS after 48h of treatment of BIBF1120-CHZ868 (left graph) and BIBF1120-ruxolitinib (right graph) combinations. Viability was assessed from apoptosis and necrosis after staining with Annexin V-PE/7AAD and expressed as decrease of the percentage of hCD10$^+$ viable blasts (Annexin V-PE/7AAD double negative cells) and expressed as percentage of viability on untreated cells. N=3 experiments, in

technical duplicate. Error bars represent standard deviation. The internal control is represented by untreated (ut) cells. Student's T test is shown as p values: *p<0.05; **p<0.01; ***p<0.001.

Figure 2. High throughput drug screening with co-culture validation on PDXs carrying *JAK2* rearrangements and *in-vivo* CHZ868 targeting of xenotransplanted NSG mice with blasts carrying *JAK2* rearrangements. A. Unsupervised clustering of n=4 JAK2r blasts, one positive control (MUTZ5 cell line) and 6 healthy controls (n=3 T-cells, n=3 PBMCs) expressing their drug sensitivity score (DSS) values. DSS reported values are proportional to the efficacy of a group of standard chemotherapy drugs currently used in the AIEOP BFM 2017 protocol, a group of inhibitors known to target JAK, in addition to venetoclax and obatoclax (BLC2i) and omaveloxolone (NFKBi). Box plots represent the mean DSS ± SD distribution among the samples for each column. **B.** *Ex-vivo* viability of hCD10+ PDX-derived blasts on HBMS co-culture after 48h drugs combinations of AT9283 and CHZ868, tested at three different dosages including their patient specific LD50s, on *PAX5::JAK2* PDX-derived blasts. Viability was assessed from apoptosis and necrosis after staining with Annexin V-PE/7AAD and expressed as decrease of the percentage of $hCD10^+$ viable blasts (Annexin V-PE/7AAD double negative cells) and expressed as percentage of viability on untreated cells. N=3 experiments, in technical duplicate. Error bars represent standard deviation. The internal control is represented by untreated (ut) cells. Student's T test is shown as p values: *p<0.05; **p<0.01; ***p<0.001; ****p<0.0001. **C.** Evaluation of the safety/toxicity of standard chemotherapy, JAK inhibitors, BCL2 inhibitors and NF-kB inhibitors on $CD34^+$ hematopoietic stem cells (HPSCs) purified from N=3 healthy donors, expressed as DSS value. DSS<10 was set as a stringent cut-off for no-toxicity. **D**. Evaluation of the reduction of the percentage of $hCD10^+CD19^+$ leukemic blasts in CHZ868-treated NSG mice compared to vehicle-treated mice, in bone marrow, spleen, peripheral blood and meninges of central nervous system (CNS), and reduction of spleen weight, in the setting of *PAX5::JAK2* fusion. At least N=5 mice for each group, treated for 10 days with washout on the weekend. Error bars represent standard deviation. Student's T test is shown as p values: *p<0.05; **p<0.01; ***p<0.001, ****p<0.0001, *****p<0.00001.

Figure 3. Pathways enrichment and differential gene expression analyses in CHZ868-treated mice. A. KEGG pathway gene set enrichment analysis (GSEA) performed on transcriptomic data from CHZ868-treated mice. The dot plots display significantly activated (left column) or suppressed (right column) pathways expressed by gene ratio based on normalized enriched score (NES<0 downregulation, NES>0 upregulation) and ranked by adjusted p-value (color scale), with dot size representing the number of genes per pathway (count). Pathways with adjusted stringent p-value<0.02 were considered significantly enriched. Gene set enrichment analysis (GSEA) was performed using the R clusterProfiler package. **B.** Hallmark pathway gene set enrichment analysis (GSEA) performed on transcriptomic data from CHZ868-treated mice. The dot plots display significantly activated (left column) or suppressed (right column) pathways expressed by gene ratio based on normalized enriched score (NES<0 downregulation, NES>0 upregulation) and ranked by adjusted p-value (color scale), with dot size representing the number of genes per pathway (count). Pathways with adjusted p-value<0.05 were considered significantly enriched. Gene set enrichment analysis (GSEA) was performed using the R clusterProfiler package. **C.** Differential gene expression analysis between CHZ868-treated mice (box plots in red, 4 samples each) and vehicle-treated mice (box plots in blue, 4 samples each) on genes associated with proliferation. Six of the top significantly upregulated and downregulated genes (adjusted p-value<0.05), with expression levels represented as $\log_2$(FPKM+1), are reported in the figure. P-values are derived from permutation-based Wilcoxon tests (10,000 permutations). **D.** Differential gene expression analysis between CHZ868-treated mice (box

plots in red, 4 samples each) and vehicle-treated mice (box plots in blue, 4 samples each) on genes associated with NF-kB pathway. Nine of the top significantly upregulated and downregulated genes (adjusted p-value<0.05), with expression levels represented as $\log_2$(FPKM+1), are reported in the figure. P-values are derived from permutation-based Wilcoxon tests (10,000 permutations).

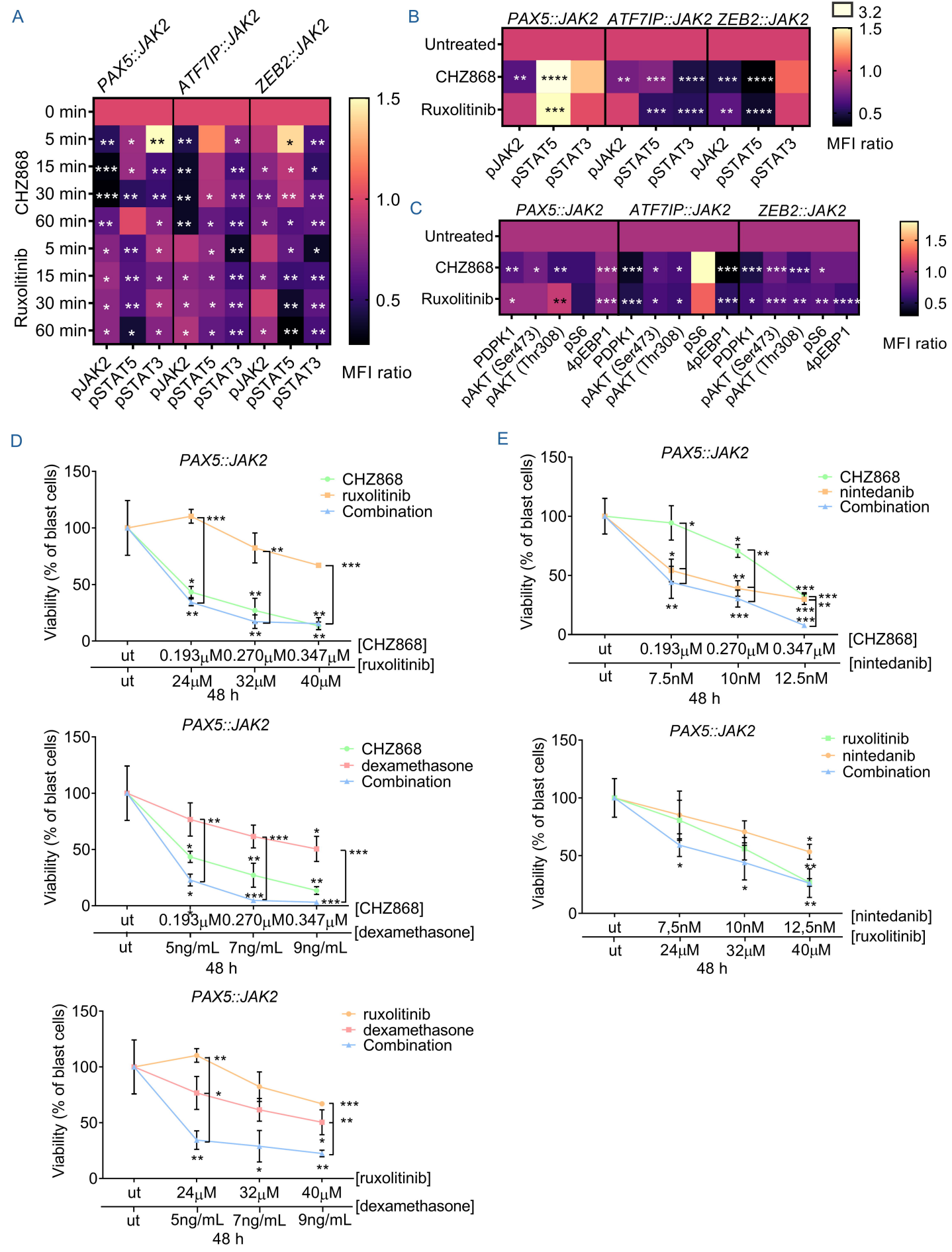
A
PAX5::JAK2
ATF7IP::JAK2
ZEB2::JAK2
CHZ868
Ruxolitinib
0 min
5 min
15 min
30 min
60 min
pJAK2
pSTAT5
pSTAT3
MFI ratio
B
Untreated
CHZ868
Ruxolitinib
C
PDPK1
pAKT (Ser473)
pAKT (Thr308)
pS6
4pEBP1
D
Viability (% of blast cells)
CHZ868
ruxolitinib
Combination
[CHZ868]
[ruxolitinib]
ut
0.193μM
0.270μM
0.347μM
24μM
32μM
40μM
48 h
dexamethasone
5ng/mL
7ng/mL
9ng/mL
[dexamethasone]
E
nintedanib
7.5nM
10nM
12.5nM
[nintedanib]
7,5nM
12,5nM

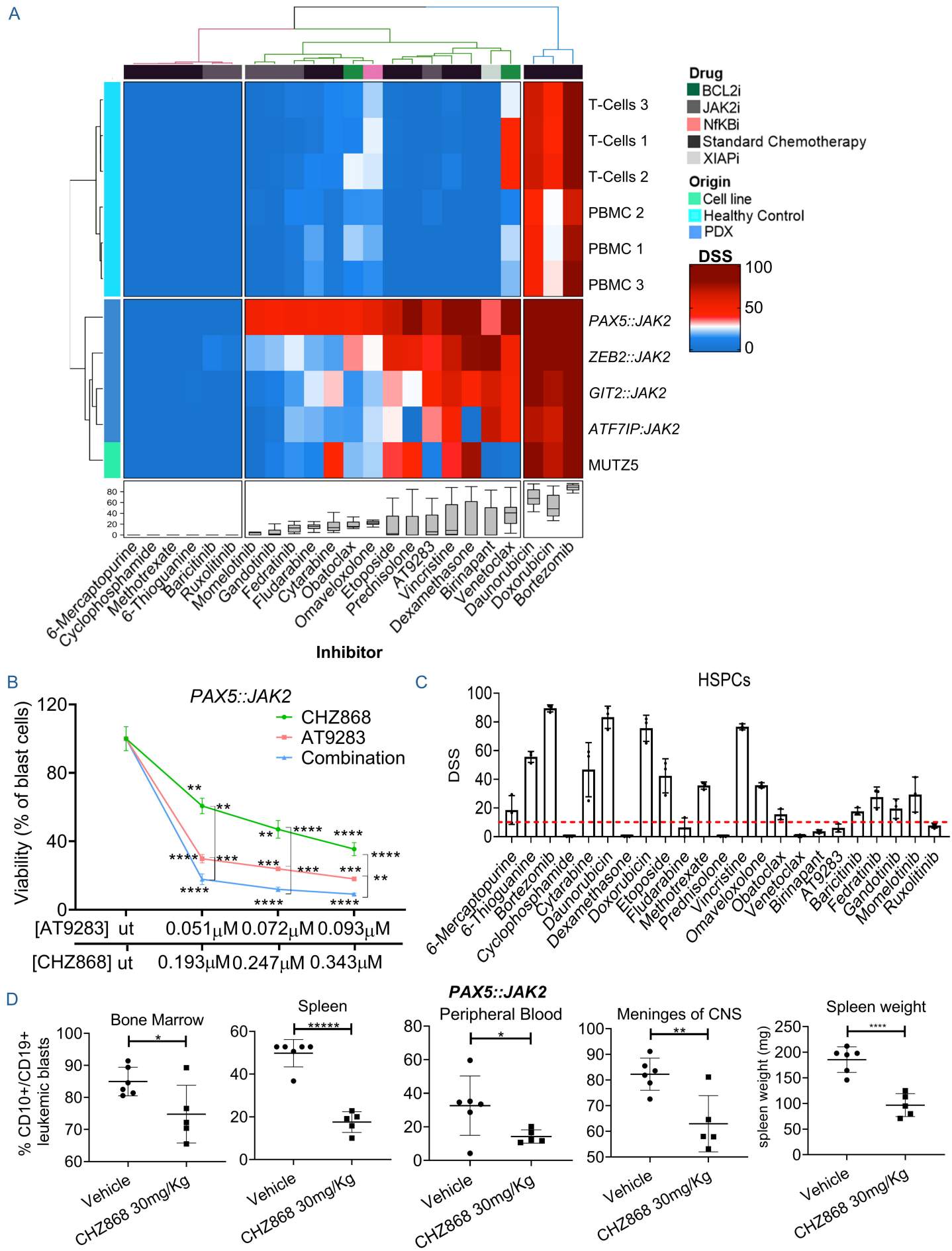
A
T-Cells 3
T-Cells 1
T-Cells 2
PBMC 2
PBMC 1
PBMC 3
PAX5::JAK2
ZEB2::JAK2
GIT2::JAK2
ATF7IP:JAK2
MUTZ5
Drug
BCL2i
JAK2i
NfKBi
Standard Chemotherapy
XIAPi
Origin
Cell line
Healthy Control
PDX
DSS
100
50
0
6-Mercaptopurine
Cyclophosphamide
Methotrexate
6-Thioguanine
Baricitinib
Ruxolitinib
Momelotinib
Gandotinib
Fedratinib
Fludarabine
Cytarabine
Obatoclax
Omaveloxolone
Etoposide
Prednisolone
AT9283
Vincristine
Dexamethasone
Birinapant
Venetoclax
Daunorubicin
Doxorubicin
Bortezomib
Inhibitor
B
PAX5::JAK2
CHZ868
AT9283
Combination
Viability (% of blast cells)
[AT9283] ut 0.051μM 0.072μM 0.093μM
[CHZ868] ut 0.193μM 0.247μM 0.343μM
C
HSPCs
DSS
D
PAX5::JAK2
Bone Marrow
% CD10+/CD19+ leukemic blasts
Spleen
Peripheral Blood
Meninges of CNS
Spleen weight
spleen weight (mg)
Vehicle
CHZ868 30mg/Kg

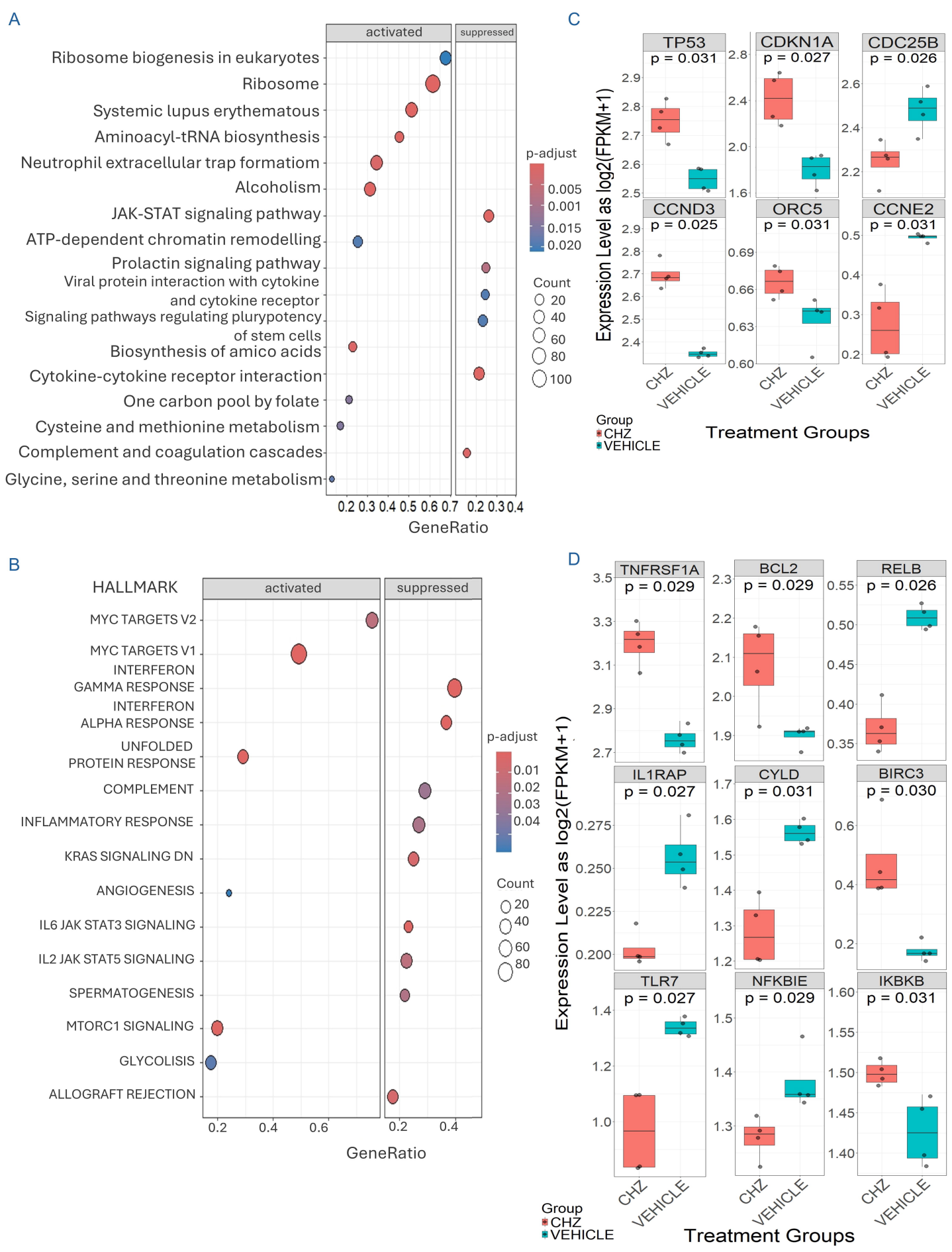
A
activated
suppressed
Ribosome biogenesis in eukaryotes
Ribosome
Systemic lupus erythematous
Aminoacyl-tRNA biosynthesis
Neutrophil extracellular trap formatiom
Alcoholism
JAK-STAT signaling pathway
ATP-dependent chromatin remodelling
Prolactin signaling pathway
Viral protein interaction with cytokine and cytokine receptor
Signaling pathways regulating plurypotency of stem cells
Biosynthesis of amico acids
Cytokine-cytokine receptor interaction
One carbon pool by folate
Cysteine and methionine metabolism
Complement and coagulation cascades
Glycine, serine and threonine metabolism
0.2 0.3 0.4 0.5 0.6 0.7
0.2 0.3 0.4
GeneRatio
p-adjust
0.005
0.001
0.015
0.020
Count
20
40
60
80
100
C
TP53
p = 0.031
CDKN1A
p = 0.027
CDC25B
p = 0.026
CCND3
p = 0.025
ORC5
p = 0.031
CCNE2
p = 0.031
Expression Level as log2(FPKM+1)
CHZ
VEHICLE
Group
CHZ
VEHICLE
Treatment Groups
B
HALLMARK
activated
suppressed
MYC TARGETS V2
MYC TARGETS V1
INTERFERON GAMMA RESPONSE
INTERFERON ALPHA RESPONSE
UNFOLDED PROTEIN RESPONSE
COMPLEMENT
INFLAMMATORY RESPONSE
KRAS SIGNALING DN
ANGIOGENESIS
IL6 JAK STAT3 SIGNALING
IL2 JAK STAT5 SIGNALING
SPERMATOGENESIS
MTORC1 SIGNALING
GLYCOLISIS
ALLOGRAFT REJECTION
0.2 0.4 0.6
0.2 0.4
GeneRatio
p-adjust
0.01
0.02
0.03
0.04
Count
20
40
60
80
D
TNFRSF1A
p = 0.029
BCL2
p = 0.029
RELB
p = 0.026
IL1RAP
p = 0.027
CYLD
p = 0.031
BIRC3
p = 0.030
TLR7
p = 0.027
NFKBIE
p = 0.029
IKBKB
p = 0.031
Expression Level as log2(FPKM+1)
CHZ
VEHICLE
Group
CHZ
VEHICLE
Treatment Groups

A

Patient	Age	Phenotype	Blasts %	MRD Stratification	Protocol	JAK2R or CRLF2r	JAK2 mutational Status	Karyotype
Patient 1	2	B-II	80	medium risk	2009	chr9::chr9PAX5::JAK2	JAK2 wt	nk
Patient 2	6	B-II	nk	medium risk	2009	chr9::chr12 ATF7IP::JAK2	JAK2 wt	nk
Patient 3	16	B-II	nk	medium risk	2000-R2006	chr2::chr9 ZEB2::JAK2	JAK2 wt	nk
Patient 4	11	B-II	89	high risk	2017	chr9::chr12 GIT2::JAK2	JAK2 wt	nk
Patient 5	2	B-II	60	standard risk	2017	chr9::chr9PAX5::JAK2	JAK2 wt	nk
Patient 6	14	B-II	70	early high risk	2017	chr9::chr9PAX5::JAK2	JAK2 wt	46,X,der(Y)(Ypter->Yq12::Y::Yq12->Yqter)[30]
Patient 7	17	B-II	80	high risk	2017	chr9::chr9PAX5::JAK2	JAK2 wt	nucish9p34(ABLx2),22q11.2 (BCRx2),11q23(MLLx2)(200),(ETV6x1),(RUNX1x2)(ETV6 withRUNX1 x0)(120/200)
Patient 8	4	B-II	82	early high risk	2017	chr9::chr9PAX5::JAK2	JAK2 wt	nk
Patient 9	12	B-II	95	high risk	2017	chr9::chr9PAX5::JAK2	JAK2 wt	nk
Patient 10	15	B-II	53	high risk	2009	chr9::chr9TLE4::JAK2	JAK2 wt	nk
Patient 11	4	B-II	87	medium risk	2017	chr9::chr22 BCR::JAK2	JAK2 wt	46,XX,+X,del(9)(p13p21),idic(17)(p11),-21[8]/46,XX[2]
Patient 12	12	B-II	60	standard risk	2017	chr9::chr17 MPRIP::JAK2	JAK2 wt	nk
Positive control 1	4	B-II	85	intermediate risk	2009	P2RY8::CRLF2	JAK2 wt	nk (patient affected by Down syndrome)
Positive control 2	4	B-II	85	standard risk	2009	P2RY8::CRLF2	JAK2 *Lc81-Ic82 insEA* mutation	47,XY,+21c[20]
Negative control 1	16	B-III	95	intermediate risk	2009	absent	JAK2 wt	nk
Negative control 2	3	B-II	93	standard risk	2009	absent	JAK2 wt	nk

B

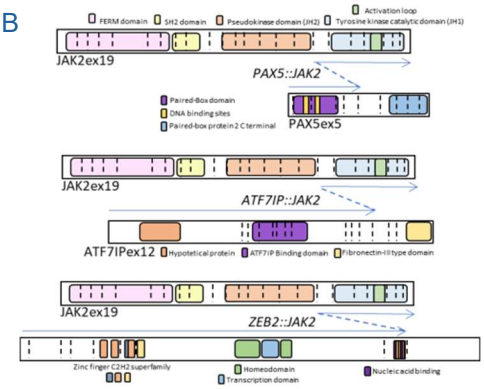

C

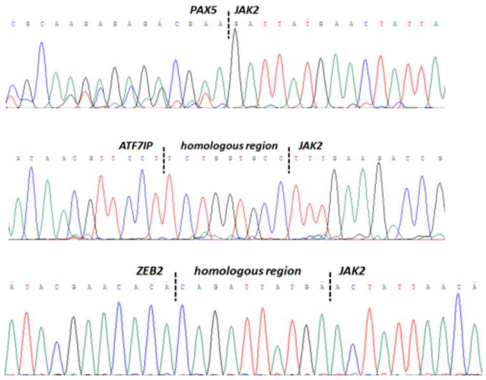

D

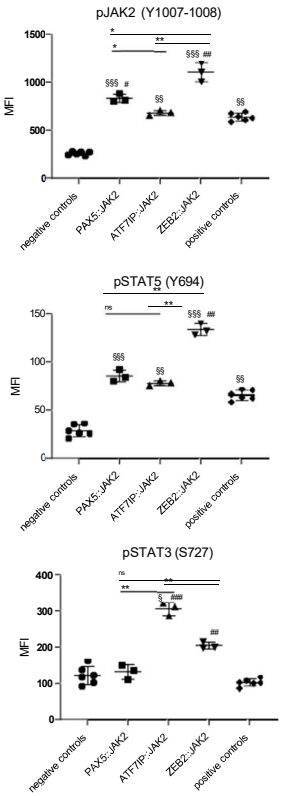

E

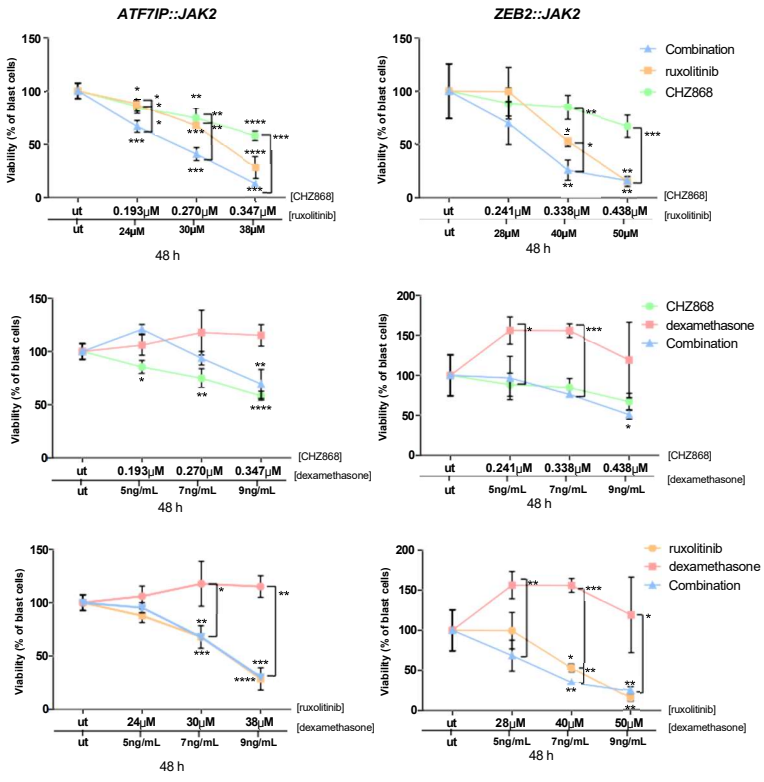

F

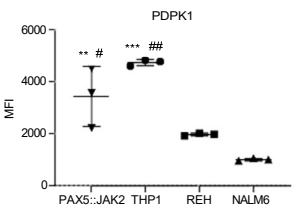

G

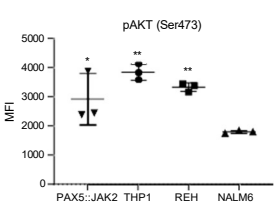

H

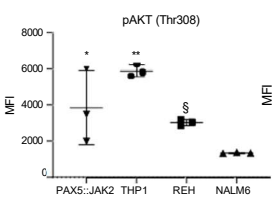

I

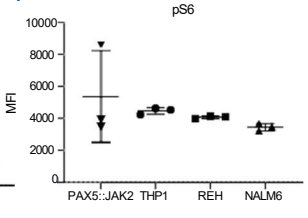

L

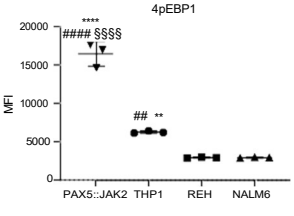

Supplementary figure 1. Molecular and functional characterization of *JAK2* rearranged patient cohort and downstream signaling activity (A-L). A. Cohort of JAK2r patients (patients 1-12), positive controls and negative controls identified by NGS, with summary of their main clinical characteristics, indication of the *JAK2* or *CRLF2* fusion gene, *JAK2* mutational status and karyotype. Blasts from patients 1-3 (highlighted in blue) are the ones used for the *ex-vivo* and *in-vivo* experiments. nk = not known. **B-C.** Representation of the fusion breakpoints of *PAX5::JAK2*, *ATF7IP::JAK2* and the novel *ZEB2::JAK2*, each maintaining *JAK2* tyrosine kinase catalytic domain at the end of the fusion gene, with indication of the exons and corresponding protein domains (**B**), and corresponding sanger sequences (**C**). **D**. Basal level of phosphorylation of pJAK2 (Y1007-1008), pSTAT5 (Y694), pSTAT3 (S727) of the three patients carrying JAK2r (*PAX5::JAK2, ATF7IP::JAK2, ZEB2::JAK2*) compared to n=2 positive controls, carrying one a *CRLF2* rearrangement and a $JAK2_{R683G}$ mutation, and one carrying only a *CRLF2* rearrangement, and compared to n=2 negative controls. N=3 experiments. Error bars represent standard deviation. Student's T test is shown as p values: *p<0.05; **p<0.01, ***p<0.001 among JAK2r, §p<0.05; §§p<0.01, §§§p<0.001 versus negative controls, #p<0.05; ##p<0.01, ###p<0.001 versus positive controls. **E.** *Ex-vivo* viability of $hCD10^+$ PDX-derived blasts on HBMS co-culture after 48h drugs combinations on *ATF7IP::JAK2* positive blasts (left column), indicating the decrease of viable blasts while increasing the dosages (CHZ868: 0.193µM, 0.270µM, 0.347µM; ruxolitinib: 24µM, 30µM, 38µM; dexamethasone: 5ng/mL, 7ng/mL, 9ng/mL) and on *ZEB2::JAK2* positive blasts (right column), indicating the decrease of viable blasts while increasing the dosages (CHZ868: 0.241µM, 0.338µM, 0.438µM; ruxolitinib: 28µM, 40µM, 50µM; dexamethasone: 5ng/mL, 7ng/mL, 9ng/mL). Viability was assessed from apoptosis and necrosis after staining with Annexin V-PE/7AAD and expressed as decrease of the percentage of $hCD10^+$ viable blasts (Annexin V-PE/7AAD double negative cells) and expressed as percentage of viability on untreated cells. N=3 experiments, in technical duplicate. Error bars represent standard deviation. Each column represents results on one fusion setting. The internal control is represented by untreated (ut) cells. Student's T test is shown as p values: *p<0.05; **p<0.01; ***p<0.001, ****p<0.0001. **F-L.** Basal level evaluation of the phosphorylation of PI3K-AKT pathway effectors PDPK1 (**F**), pAKT (S473) (**G**), pAKT (T308) (**H**), 4pEBP1 (**I**), pS6 (**L**), compared to THP1 and REH cell lines (high PI3K-AKT pathway expressing cells) and NALM6 cell lines (low PI3K-AKT pathway expressing cells) evaluated by phosphoflow and expressed as basal MFI. N=3 experiments. Error bars represent standard deviation. Student's T test is shown as p values: *p<0.05; **p<0.01, ***p<0.001 versus NALM6, §p<0.05; §§p<0.01, §§§p<0.001 versus THP1, #p<0.05; ##p<0.01, ###p<0.001 versus REH.

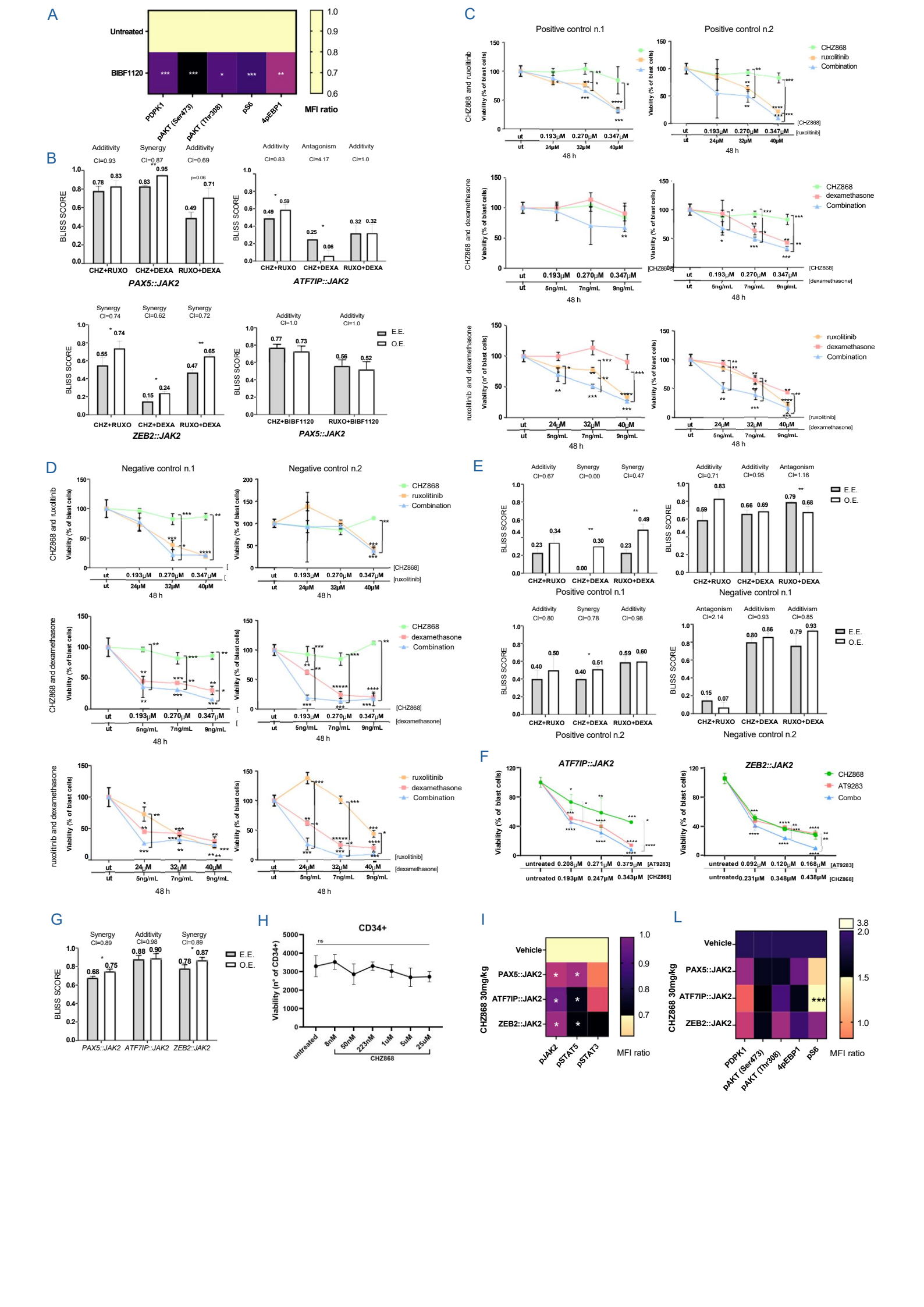
A
Untreated
BIBF1120
PDPK1
pAKT (Ser473)
pAKT (Thr308)
pS6
4pEBP1
MFI ratio
B
BLISS SCORE
CHZ+RUXO
CHZ+DEXA
RUXO+DEXA
PAX5::JAK2
ATF7IP::JAK2
ZEB2::JAK2
CHZ+BIBF1120
RUXO+BIBF1120
E.E.
O.E.
C
Positive control n.1
Positive control n.2
CHZ868 and ruxolitinib
CHZ868 and dexamethasone
ruxolitinib and dexamethasone
Viability (% of blast cells)
CHZ868
ruxolitinib
dexamethasone
Combination
48 h
D
Negative control n.1
Negative control n.2
E
Positive control n.1
Negative control n.1
Positive control n.2
Negative control n.2
F
ATF7IP::JAK2
ZEB2::JAK2
AT9283
Combo
G
H
CD34+
Viability (n° of CD34+)
CHZ868
I
Vehicle
PAX5::JAK2
ATF7IP::JAK2
ZEB2::JAK2
CHZ868 30mg/kg
pJAK2
pSTAT5
pSTAT3
MFI ratio
L
PDPK1
pAKT (Ser473)
pAKT (Thr308)
4pEBP1
pS6

Supplementary figure 2. Drug combination effects and signaling inhibition in *JAK2* rearranged models (A-L). A. Heatmap expressing the mean fluorescence intensity of PI3K-AKT pathway effectors PDPK1, pAKT (S473), pAKT (T308), 4pEBP1, pS6, of 48h BIBF1120-treated *PAX5::JAK2* blasts seeded on HBMS compared to untreated blasts, evaluated by phosphoflow and expressed as MFI ratios of treated on untreated $hCD10^+$ blasts. N=3 experiments. Error bars represent standard deviation. Student's T test is shown as p values: *p<0.05; **p<0.01, ***p<0.001. **B.** 50% lethal dose **(**LD50) bliss score of the combinations of pairs of the drugs (CHZ868, CHZ; ruxolitinib, RUXO; dexamethasone, DEXA; nintedanib, BIBF1120) after 48h of treatment, indicating the ratio of apoptotic treated blasts versus untreated, which compares expected event (E.E.) and observed event (O.E.), with indication of combination index (CI) values, to evaluate synergy (p value and CI<1), additivity (no p value and CI≤0) or antagonism (CI>1). **C-D.** *Ex-vivo* apoptosis/viability assays of the combination of pairs of drugs, given at three different dosages, on primary blasts of positive controls (**C**) and negative controls (**D**), treated for 48h in co-culture on HBMS. Viability was assessed from apoptosis and necrosis after staining with Annexin V-PE/7AAD and expressed as decrease of the percentage of $hCD10^+$ viable blasts (Annexin V-PE/7AAD double negative cells) with increasing dosages of drugs. N=3 experiments, in technical duplicate. Error bars represent standard deviation. The internal control is represented by untreated (ut) cells. Student's T test is shown as p values: *p<0.05; **p<0.01; ***p<0.001, ****p<0.0001. **E**. LD50 bliss score of the combinations of pairs of the drugs (CHZ868, CHZ; ruxolitinib, RUXO; dexamethasone, DEXA), comparing expected event (EE) and observed event (OE), with indication of the combination index (CI) values, to evaluate synergy (p value and CI<1), additivity (no p value, CI≤0) or antagonism (CI>1). **F.** *Ex-vivo* viability of $hCD10^+$ PDX-derived blasts on HBMS co-culture after 48h drugs combinations of AT9283 and CHZ868, tested at three different dosages including their patient specific LD50s, on *ATF7IP::JAK2* (left graph) and *ZEB2::JAK2* (right graph) PDX-derived blasts. Viability was assessed from apoptosis and necrosis after staining with Annexin V-PE/7AAD and expressed as decrease of the percentage of $hCD10^+$ viable blasts (Annexin V-PE/7AAD double negative cells) and expressed as percentage of viability on untreated cells. N=3 experiments, in technical duplicate. Error bars represent standard deviation. The internal control is represented by untreated (ut) cells. Student's T test is shown as p values: *p<0.05; **p<0.01; ***p<0.001; ****p<0.0001. **G**. LD50 bliss score of the AT9283-CHZ868 combination, indicating the ratio of apoptotic treated blasts versus untreated, which compares expected event (E.E.) and observed event (O.E.), with indication of combination index (CI) values, to evaluate synergy (p value and CI<1), additivity (no p value, CI≤0) or antagonism (CI>1). **H.** Assessment of the safety of CHZ868 treatment at 6 dosages from 8nM to 25µM on $CD34^+$ hematopoietic stem cell (HSPCs) purified from healthy donors as determined by the absence of significant apoptosis induction by annexin V/7AAD staining. N=3 experiments, in technical duplicate. Error bars represent standard deviation. Student's T test expressed as p values: *p<0.05; **p<0.01; ***p<0.001, ****p<0.0001, *****p<0.00001. The internal control is represented by untreated cells. **I-L**. Heatmaps reporting the reduction of phosphorylation of pJAK2 (Y1007-1008), pSTAT5 (Y694) and pSTAT3 (S727) after 30mg/Kg CHZ868 *in-vivo* treatment of *PAX5::JAK2* fusion setting, of *ATF7IP::JAK2* fusion setting and of *ZEB2::JAK2* fusion setting, represented as MFI ratios on vehicle treated mice (**I**), and reporting the reduction of phosphorylation of PI3K-AKT pathway effectors [PDPK1, pAKT (S473), pAKT (T308), 4pEBP1, pS6] after 30mg/Kg CHZ868 *in-vivo* treatment of *PAX5::JAK2* setting, of *ATF7IP::JAK2* fusion setting and of *ZEB2::JAK2* fusion setting represented as MFI ratios on vehicle treated mice (**L**). At least N=5 mice per group. Student's T test expressed as p values: *p<0.05; **p<0.01; ***p<0.001. The internal control is represented by vehicle-treated mice. Statistics reported in white refers to a significant reduction of phosphorylation in CHZ868-treated mice compared to vehicle-treated mice, while statistics reported in black refers to a significant increase of phosphorylation in CHZ868-treated mice compared to vehicle-treated mice.

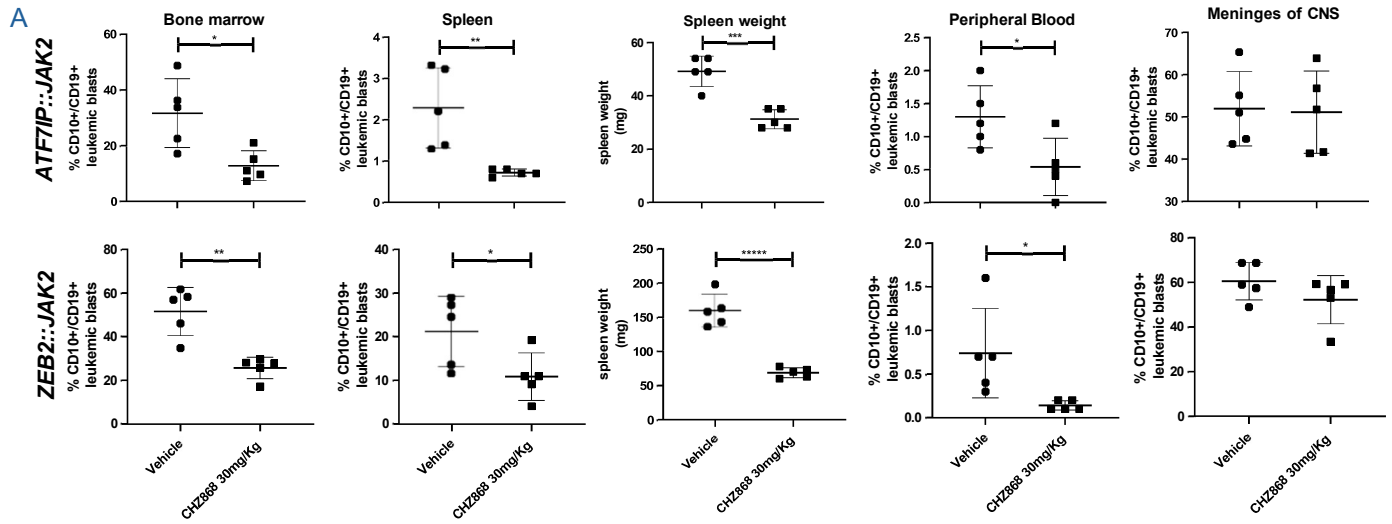
A
Bone marrow
Spleen
Spleen weight
Peripheral Blood
Meninges of CNS
ATF7IP::JAK2
ZEB2::JAK2
% CD10+/CD19+ leukemic blasts
spleen weight (mg)
Vehicle
CHZ868 30mg/Kg

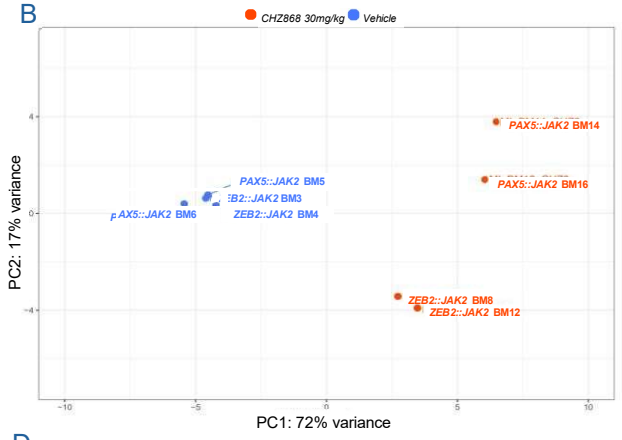
B
CHZ868 30mg/kg
Vehicle
PAX5::JAK2 BM14
PAX5::JAK2 BM16
PAX5::JAK2 BM5
ZEB2::JAK2 BM3
PAX5::JAK2 BM6
ZEB2::JAK2 BM4
ZEB2::JAK2 BM8
ZEB2::JAK2 BM12
PC2: 17% variance
PC1: 72% variance

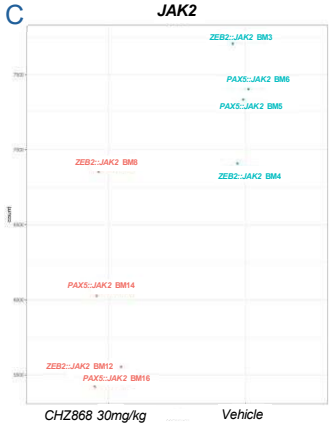
C
JAK2
CHZ868 30mg/kg
Vehicle

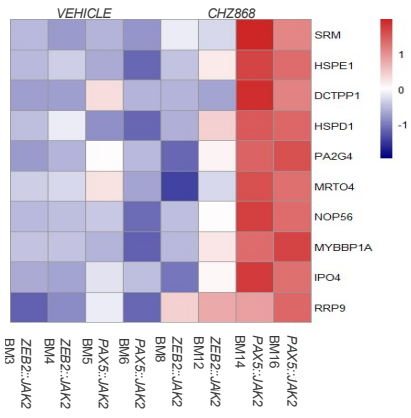
F
VEHICLE
CHZ868
SRM
HSPE1
DCTPP1
HSPD1
PA2G4
MRTO4
NOP56
MYBBP1A
IPO4
RRP9

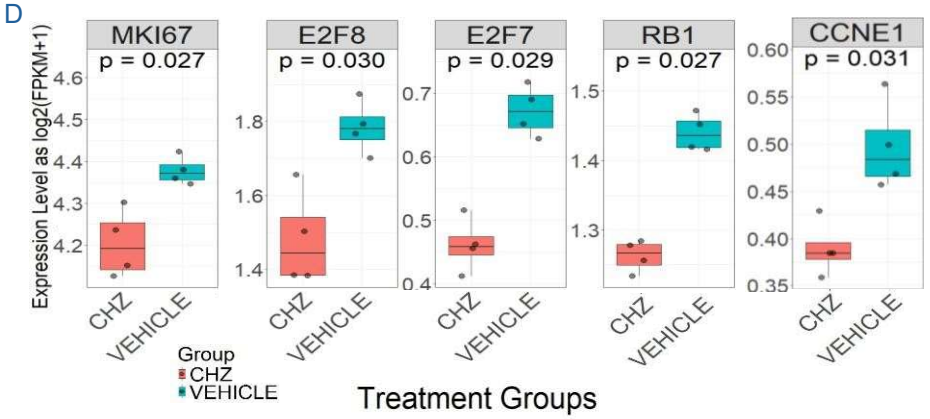
D
MKI67
p = 0.027
E2F8
p = 0.030
E2F7
p = 0.029
RB1
p = 0.027
CCNE1
p = 0.031
Expression Level as log2(FPKM+1)
CHZ
VEHICLE
Group
CHZ
VEHICLE
Treatment Groups

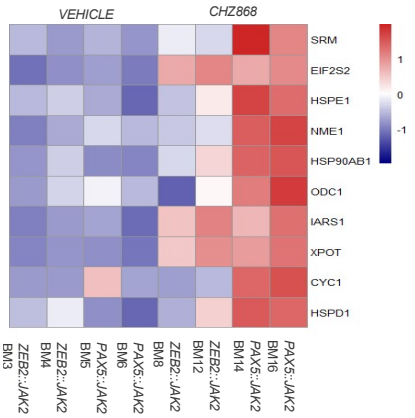
VEHICLE
CHZ868
SRM
EIF2S2
HSPE1
NME1
HSP90AB1
ODC1
IARS1
XPOT
CYC1
HSPD1

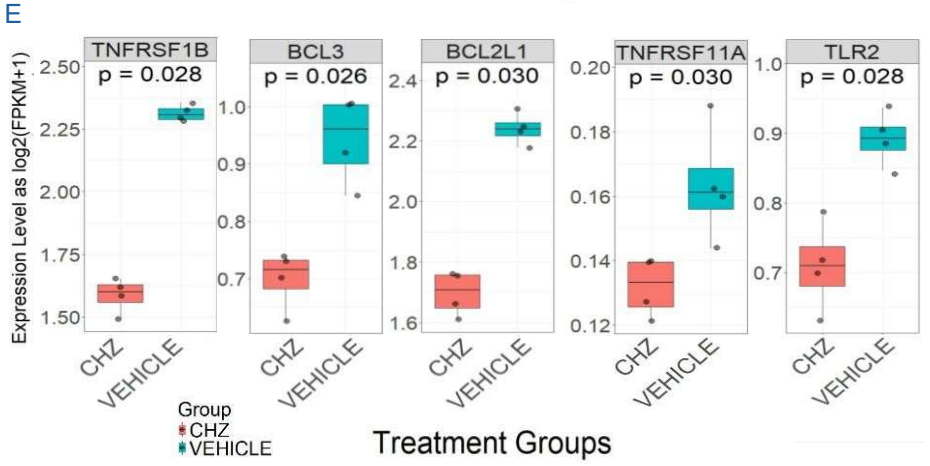
E
TNFRSF1B
p = 0.028
BCL3
p = 0.026
BCL2L1
p = 0.030
TNFRSF11A
p = 0.030
TLR2
p = 0.028
Expression Level as log2(FPKM+1)
CHZ
VEHICLE
Group
CHZ
VEHICLE
Treatment Groups

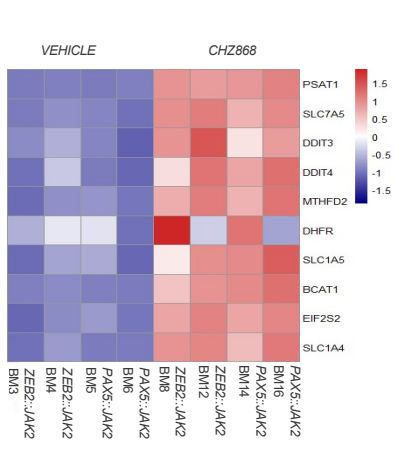
VEHICLE
CHZ868
PSAT1
SLC7A5
DDIT3
DDIT4
MTHFD2
DHFR
SLC1A5
BCAT1
EIF2S2
SLC1A4

Supplementary figure 3. CHZ868 *in-vivo* efficacy and consequent transcriptional profiling and pathway modulation in CHZ868-treated mice (A-F). A. Evaluation of the reduction of the percentage of $hCD10^{+}CD19^{+}$ leukemic blasts in CHZ868-treated NSG mice compared to vehicle-treated mice, in bone marrow, spleen, peripheral blood and meninges of central nervous system (CNS), and reduction of spleen weight, in the setting of *ATF7IP::JAK2* fusion (upper row) and of *ZEB2::JAK2* fusion (lower row). At least N=5 mice for each group, treated for 10 days with washout on the weekend. Error bars represent standard deviation. Student's T test is shown as p values: *p<0.05; **p<0.01; ***p<0.001, ****p<0.0001, *****p<0.00001. **B**. Principal Component Analysis (PCA) based on gene expression profiles on n=8 samples, including n=4 vehicle-treated (blue dots) and n=4 CHZ868-treated (red dots) extracted RNA from blasts of *in-vivo* treated mice. Separation along the principal components reflects transcriptional differences induced by the treatment. **C.** *JAK2* downregulation in *in-vivo* CHZ868-treated mice (left column, red dots) compared to the higher *JAK2* expression in vehicle-treated mice (right column, blue dots) obtained by whole transcriptome analysis. **D**. Differential gene expression analysis between CHZ868-treated mice (box plots in red, 4 samples each) and vehicle-treated mice (box plots in blue, 4 samples each) on genes associated with proliferation. Five of the top significantly upregulated and downregulated genes (adjusted p-value< 0.05), with expression levels represented as $\log_2(FPKM+1)$, are reported in the figure. p-values derived from permutation-based Wilcoxon tests (10,000 permutations). **E**. Differential gene expression analysis between CHZ868-treated mice (box plots in red, 4 samples each) and vehicle-treated mice (box plots in blue, 4 samples each) on genes associated with NF-kB pathway. Five of the top significantly upregulated and downregulated genes (adjusted p-value < 0.05), with expression levels represented as $\log_2(FPKM+1)$, are reported in the figure. p-values derived from permutation-based Wilcoxon tests (10,000 permutations). **F**. Scaled expression of the top 10 genes in each hallmark [MYC V1 (upper heatmap), MYC V2 (central column), MTORC1 (right column)], sorted between-groups variance, which resulted to be correlated to a metabolic rewiring inside blasts from CHZ868-treated mice compared to blasts from vehicle-treated mice.